Removal of iron from drinking water by electrocoagulation: Adsorption and kinetics studies

Subramanyan Vasudevan[†], Jeganathan Jayaraj, Jothinathan Lakshmi, and Ganapathy Sozhan

Central Electrochemical Research Institute (CSIR), Karaikudi 630 006, India

Abstract−The present study provides an electrocoagulation process for the removal of iron from drinking water with aluminum alloy as the anode and stainless steel as the cathode. The studies were carried out as a function of pH, temperature and current density. The adsorption capacity was evaluated with both the Langmuir and the Freundlich isotherm models. The results showed that the maximum removal efficiency of 98.8% was achieved at a current density of 0.06 A dm^{-2}, at a pH of 6.5. The adsorption of iron preferably fitting the Langmuir adsorption isotherm suggests monolayer coverage of adsorbed molecules. The adsorption process follows second-order kinetics. Temperature studies showed that adsorption was endothermic and spontaneous in nature.

Key words: Iron, Removal, Electrocoagulation, Adsorption, Kinetics
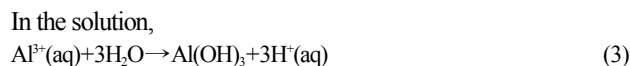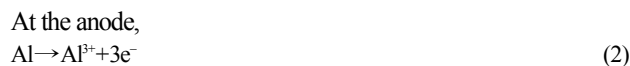
INTRODUCTION

The presence of iron is probably the most common water problem faced by consumers and water professionals next to hardness. Iron is commonly present in ground water worldwide. In India, severe groundwater contamination by iron has been reported [1-4] by several states like Andhra Pradesh, Assam, Bhubaneswar, Chhattisgarh, Karnataka and Orrisa. Localized pockets are observed in states like Bihar, Jharkhand, Kerala, Maharastra, Madhya Pradesh, North Eastern States, Punjab, Rajasthan, Tamilnadu and Uttar Pradesh. Although the presence of iron in the drinking water is not harmful to human health, it is undesirable. Bad taste, discoloration, staining and high turbidity are some of the aesthetic problems associated with iron. Based on the above considerations, the World Health Organization (WHO) recommends that the iron contamination in drinking water should be less than 0.3 mg/L [5]. The European Commission directive recommends that the iron in water supplies should be less than 0.2 mg/L [6]. The Indian discharge limit for iron is 0.3 mg/L [7].

Iron usually exists in two oxidation states, reduced soluble divalent ferrous (Fe^{2+}) and oxidized trivalent ferric (Fe^{3+}). Several methods, namely oxidation-precipitation-filtration, lime softening, ion-exchange, activated carbon and other filtration materials, adsorption, bioremediation, supercritical fluid extraction, by aerated granular filter, sub-surface iron removal and membrane processes have been employed for iron removal from groundwater [8-15]. The most commonly used methods for the removal of iron are oxidation-precipitation-filtration, ion exchange, lime softening and membrane processes. In the case of ion exchange process the limitations like cost of resin, regeneration and waste disposal prevent the process as uneconomical. Further, the major difficulty in using this method is that if any oxidation occurs during the process the resulting precipitate can coat and foul the ion exchange media. Oxidation followed by precipitation and filtration is a relatively simple process,

but it is ineffective when the concentration of iron in the solution is high (or) the solution pH is low (or) iron is in complex form. Addition of lime leads to rises in the pH values of water up to 11-12. The limitations are very high maintenance cost and more space. Membrane process has emerged as a preferred alternative to provide safe drinking water. Due to disadvantages like high cost of membrane, brine disposal and post treatment of water prevent the process as uneconomical.

Recent research has demonstrated that electrochemistry offers an attractive alternative to the above-mentioned traditional methods for treating wastewaters [16-22]. Electrochemical coagulation, which is one of these techniques, is the electrochemical production of destabilization agents that brings about charge neutralization for pollutant removal, and it has been used for water or wastewater treatment. Usually, aluminum, zinc or iron plates are used as electrodes in the electrocoagulation process. Electrochemically generated metallic ions from these electrodes can undergo hydrolysis near the anode to produce a series of activated intermediates that are able to destabilize the finely dispersed particles present in the water/wastewater to be treated. The destabilized particles then aggregate to form flocs [23]. (i) When aluminium is used as anode, the reactions are as follows:
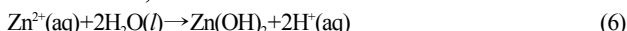
At the cathode,
$$2H_2O + 2e^- \rightarrow H_2\,(g) + 2OH^- \tag{1}$$

At the anode,
$$Al \rightarrow Al^{3+} + 3e^- \tag{2}$$

In the solution,
$$Al^{3+}(aq) + 3H_2O \rightarrow Al(OH)_3 + 3H^+(aq) \tag{3}$$

(ii) When zinc is used as anode, the reactions are as follows:

At the cathode,
$$2H_2O + 2e^- \rightarrow H_2(g) + 2OH^- \tag{4}$$

At the anode,
$$Zn \rightarrow Zn^{2+} + 2e^- \tag{5}$$

[†]To whom correspondence should be addressed.
E-mail: vasudevan65@gmail.com

In the solution,

$$Zn^{2+}(aq)+2H_2O(l) \rightarrow Zn(OH)_2+2H^+(aq) \quad (6)$$

The advantages of electrocoagulation include high particulate removal efficiency, a compact treatment facility and the possibility of complete automation. This method is characterized by reduced sludge production, a minimum requirement of chemicals, and ease of operation [24,25]. Although there are numerous reports related to electrochemical coagulation as a means of removal of many pollutants from water and wastewater, there is limited work on iron removal by the electrochemical method and its adsorption and kinetics studies. This article presents the results of the laboratory scale studies on the removal of iron using aluminium alloy and stainless steel as the anode and the cathode, respectively, by electrocoagulation process. In doing so, the equilibrium adsorption behavior is analyzed by fitting models of Langmuir and Freundlich isotherms. Adsorption kinetics of electrocoagulants is analyzed using first- and second-order kinetic models. Activation energy is evaluated to study the nature of adsorption.

MATERIALS AND METHODS

1. Cell Construction and Electrolysis

The electrolytic cell (Fig. 1) consisted of a 1.0-L Plexiglas vessel that was fitted with a poly-(vinyl chloride) (PVC) cell cover with slots to introduce the electrodes, pH sensor, a thermometer and the electrolytes. Aluminum Alloy (consisting of Zn (1-4%), In (0.006-0.025%), Fe (0.15%), Si (0-.15%) (Patented material, CECRI, India), with a surface area of 0.02 m^2 acted as the anode. The cathode was
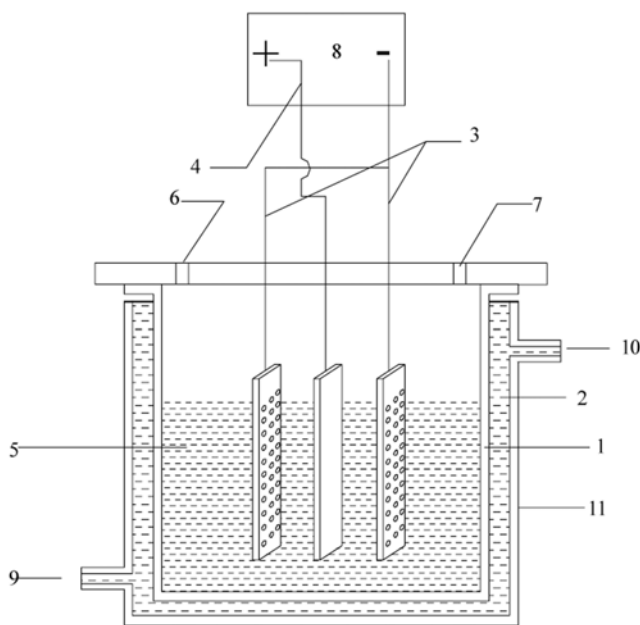

Fig. 1. Laboratory scale cell assembly.

1. Cell
2. Thermostatic water
3. Stainless steel cathode
4. Anode
5. Electrolyte
6 & 7. Holes to introduce pH sensor and thermometer

8. dc source
9. Inlet of thermostatic water
10. Outlet of thermostatic water
11. Thermostat

a stainless steel (SS 304; SAIL, India) sheet of the same size as the anode and placed at an interelectrode distance of 0.005 m. The temperature of the electrolyte was controlled to the desired value with a variation of ±2 K by adjusting the rate of flow of thermostatically controlled water through an external glass-cooling spiral. A regulated direct current was supplied from a rectifier (10 A, 0-25 V; Aplab model).

The iron (FeSO$_4$) (Analar Reagent) was dissolved in tap (drinking) water for the required concentration. A 0.90 L portion of solution was used for each experiment, which was used as the electrolyte. The pH of the electrolyte was adjusted, if required, with 1 M HCl or 1 M NaOH solutions before adsorption experiments.

2. Analysis

The concentration of iron was determined by Atomic Adsorption Spectrophotometer made by Varian, Netherlands.

The surface morphology of the anode before and after treatment was analyzed by metallurgical microscope made by ZEISS, Germany.

RESULTS AND DISCUSSION

1. Effect of Current Density

The current density is the one of the imperative operational parameters in electrocoagulation processes. To investigate the effects of current density, a series of experiments were performed using 25 mg/L iron-containing solutions, at pH 6.5, with current density being varied from 0.02 to 0.12 A dm^{-2}. The removal efficiency of iron increases rapidly up to 98.8% with a current density of 0.06 A dm^{-2} and then it remains almost constant for higher current densities as depicted in Fig. 2. According to Faraday's law [26], the current density is directly proportional to the amount of adsorbent (Aluminum hydroxide) formed, which is related to the time and current density. Hence, the amount of iron adsorption increases with the increase in adsorbent concentration, which indicates that the adsorption depends upon the availability of binding sites for iron.
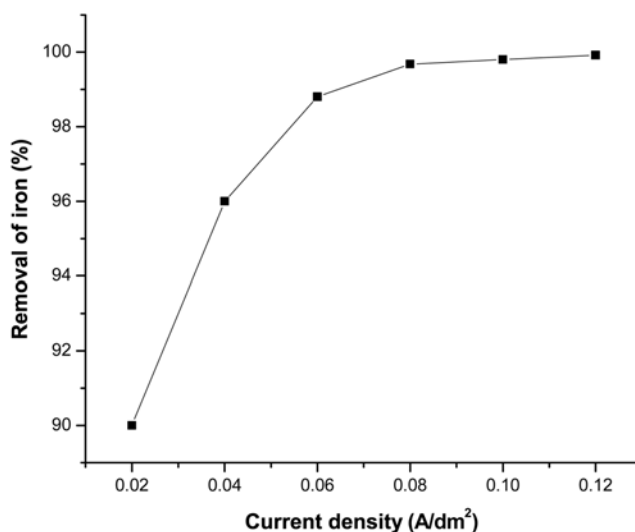

Fig. 2. Effect of current density on the removal of iron. Conditions, electrolyte pH: 6.5, concentration of iron: 25 mg/L, electrolyte temperature: 305 K.
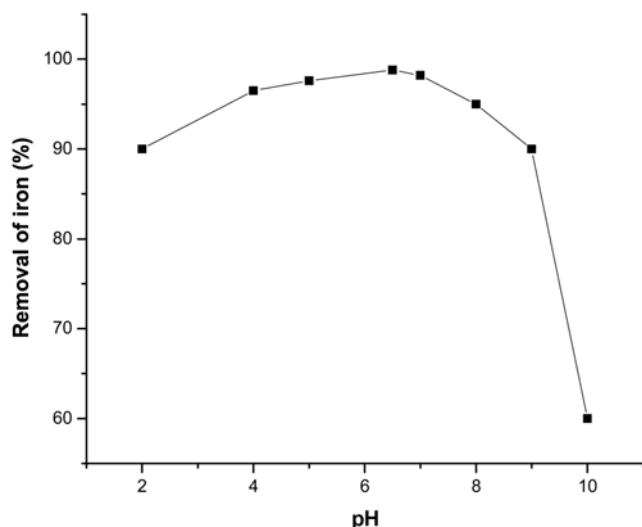
Fig. 3. Effect of pH on the removal of iron. Conditions, concentration of iron: 25 mg/L, current density: 0.06 A dm^{-2}, agitation time: 60 min, electrolyte temperature: 305 K.

2. Effect of pH

It has been established that the pH of the electrolyte is one of the important factors affecting the performance of the electrochemical process particularly on the performance of the electrocoagulation process. To evaluate its effect, a series of experiments were performed, using 25 mg/L iron-containing solution with an initial pH varying in the range 2-10. As illustrated in Fig. 3, it can be seen that the removal efficiency of iron was increased with increasing the pH, and the maximum removal efficiency of 98.8% was obtained at pH 6.5. The minimum removal efficiency of iron was 60% at pH 10.

The decrease of removal efficiency at more acidic and alkaline pH was observed by many investigators [26] and was attributed to the amphoteric behavior of Al(OH)$_3$ which leads to soluble Al^{3+} cations (at acidic pH) and to monomeric anions Al(OH)$^{4-}$ (at alkaline pH). It is well known that these soluble species are not useful for water treatment. When the initial pH was kept in neutral, all the aluminum produced at the anode formed polymeric species (Al$_{13}$O$_4$ (OH)$_{24}^{7+}$) and precipitated Al(OH)$_3$ leading to greater removal efficiency [26]. In the present study, the results agree well with the results presented in the literature, and the maximum amount of iron removal occurred at pH 6.5.

3. Effect of Initial Iron Concentration

The adsorption of iron is increased with an increase in iron concentration and remains constant after equilibrium time as depicted in Fig. 4. The equilibrium time was 25 minutes for all of the concentrations studied (5-25 mg/L). The amount of iron adsorbed (q$_e$) increased from 40.51 to 202.58 mg/g of Al(OH)$_3$, as the concentration was increased from 5 to 25 mg/L. The figure also shows that the adsorption is rapid in the initial stages and gradually decreases with progress of adsorption. The plots are single, smooth, and continuous curves leading to saturation, suggesting the possible monolayer coverage to iron on the surface of the adsorbent [27].

4. Adsorption Kinetics

The adsorption kinetic data of iron are analyzed by using the Lagergran rate equation. The first-order Lagergran model is [28],
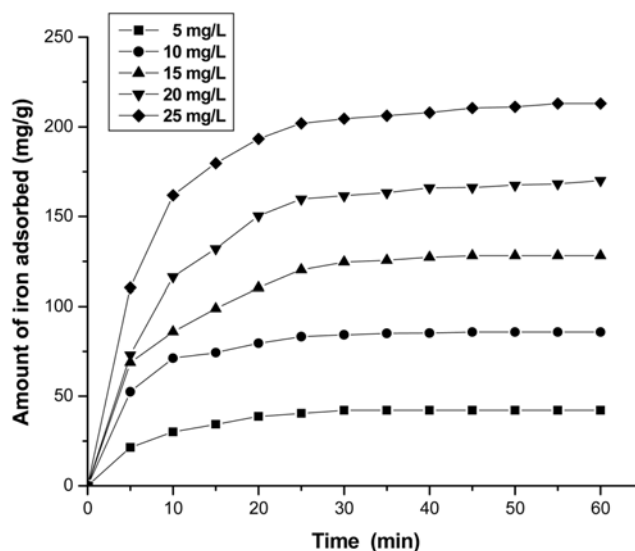
Fig. 4. Effect of agitation time and initial iron concentration on the amount of iron adsorbed. Conditions, electrolyte pH: 6.5, electrolyte temperature: 305 K, current density: 0.06 A dm^{-2}.

$$dq_t/dt = k_1 (q_e - q_t) \tag{7}$$

where q$_e$ is the amount of iron adsorbed at equilibrium, q$_t$ is the amount of iron adsorbed on the adsorbent at time t (min), and k$_1$ (min^{-1}) is the rate constant of first order adsorption. The integrated form of the above equation with the boundary conditions of t=0 to t=t and q$_t$=0 to q$_t$=q$_t$ can be written as,

$$\log(q_e - q_t) = \log q_e - k_1 t/2.303 \tag{8}$$

The q$_e$ and rate constant (k$_1$) were calculated from the slope of the plots of log (q$_e$−q$_t$) versus time (t). A straight line obtained from the plots suggests the applicability of this kinetic model. It was found that the calculated q$_e$ values do not agree with the experimental values (Table 1), so the adsorption does not obey the first-order kinetics adsorption.

The second-order kinetic model is expressed as [29],

$$dq_t/dt = k_2 (q_e - q_t)^2 \tag{9}$$

where k$_2$ is the rate constant of the second-order adsorption. The integrated form of Eq. (9) with the boundary conditions of t=0 to t=t and q$_t$=0 to q$_t$=q$_t$ can be written as

Table 1. Comparison between the experimental and calculated q$_e$ values for different initial iron concentrations in first-order adsorption isotherm at temperature 305 K and pH 6.5

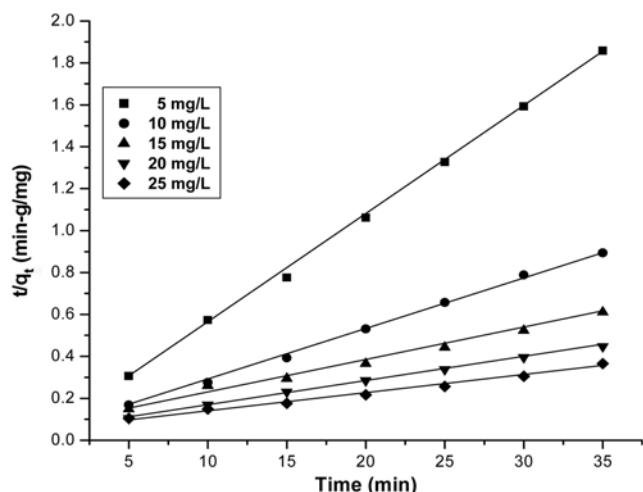| Concentration of iron (mg/L)	q$_e$ Experimental (mg/g)	k$_1$ (min g/mg)	q$_e$ Calculated (mg/g)	R^2
5	21.48	0.1330	50.11	0.9750
10	83.30	0.1147	107.13	0.9783
15	98.80	0.1086	125.36	0.9842
20	158.07	0.0742	194.86	0.9614
25	201.89	0.0724	245.18	0.9847

Fig. 5. Second-order kinetic model plot of different concentrations of iron. Conditions, electrolyte pH: 6.5, electrolyte temperature: 305 K, current density: 0.06 A dm^{-2}.

Table 2. Comparison between the experimental and calculated q_e values for different initial iron concentrations in second-order adsorption isotherm at temperature 305 K and pH 6.5

Concentration of iron (mg/L)	q_e Experimental (mg/g)	k_1 (min g/mg)	q_e Calculated (mg/g)	R^2
5	40.51	0.0026	40.57	0.9991
10	86.52	0.0021	84.65	0.9983
15	120.68	0.0014	120.19	0.9978
20	156.62	0.0012	153.84	0.9992
25	201.32	0.0009	199.22	0.9989

$$1/(q_e - q_t) = 1/q_e + k_2 t \tag{10}$$

Eq. (10) can be rearranged and linearized as,

$$t/q_t = 1/k_2 q_e^2 + t/q_e \tag{11}$$

The plot t/q_t versus time (t) (Fig. 5) shows a straight line. The second-order kinetic values of q_e and k_2 were calculated from the slope and intercept of the plots t/q_t versus t (Fig. 5). The plot shows that the correlation coefficient for the second-order kinetic model obtained in all of the concentrations studies were above 0.99, and also the calculated q_e values agree with the experimental q_e values. Table 2 depicts the computed result obtained from the second-order kinetic model. These results indicate that the adsorption system studied belongs to the second-order kinetic model. Similar phenomena have been observed in the adsorption of phosphate in Fe(III)/Cr(III) hydroxide [27].

5. Adsorption Isotherm

The adsorption capacity of the adsorbent has been tested using Freundlich [29] and Langmuir [27] isotherms. To determine the isotherms, the initial pH was kept at 6.5 and the concentration of iron used was in the range of 5-25 mg/L. The general form of the Freundlich adsorption isotherm is represented by [29]
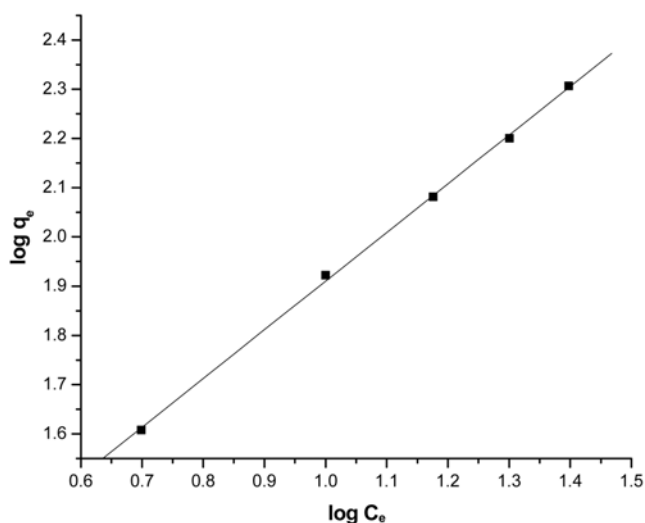

Fig. 6. Freundlich Plot (log q_e vs log C_e). Conditions, electrolyte pH: 6.5, electrolyte temperature: 305 K, current density: 0.06 A dm^{-2}.

$$q_e = KC^{1/n} \tag{12}$$

Eq. (12) can be linearized in logarithmic form, and the Freundlich constants can be determined as follows [30],

$$\text{Log } q_e = \log k_f + 1/n \log C_e \tag{13}$$

where k_f is the Freundlich constant related to adsorption capacity, n is the energy or intensity of adsorption, and C_e is the equilibrium concentration of the iron (mg/L). To determine the isotherms, the iron concentration used was 5-25 mg/L at initial pH 6.5. The Freundlich constants k_f and n values are 8.3491 (mg/g) and 0.9855 (L/mg), respectively (Fig. 6). From the analysis of the results, it is found that the Freundlich plots do not fit satisfactorily with the experimental data obtained in the present study. This agrees well with the results presented in the literature [27].

Hence, the Langmuir isotherm has been used to study the surface monolayer adsorption. The Langmuir isotherm is based on the assumption that points of valence exist on the surface of the adsorbent and that each of these sites is capable of adsorbing molecule; thus, the adsorbed layer will be one molecule thick. Furthermore, it is assumed that all the adsorption sites have equal affinities for molecules of the adsorbate and that the presence of adsorbed molecules at one site will not affect the adsorption of molecules at an adjacent site. The Langmuir isotherm is commonly expressed as [31],

$$C_e/q_e = 1/q_o b + C_e/q_o \tag{14}$$

where C_e is the concentration of the iron solution (mg/L) at equilibrium, q_e is the maximum capacity to form a complete monolayer on the surface, q_0 and b are the Langmuir constants related to adsorption capacity and free energy of adsorption. When $1/q_e$ is plotted against $1/C_e$ a straight line with slope $1/q_0 b$ is obtained, which shows the adsorption follows the Langmuir isotherm suggesting that the adsorption is apparently with monolayer coverage of adsorbed molecule as in Fig. 7. The Langmuir plot is a better fit with the experimental data compared to the Freundlich plots. The value of the adsorption capacity q_o was found to be 5.912 g/g, which is higher than
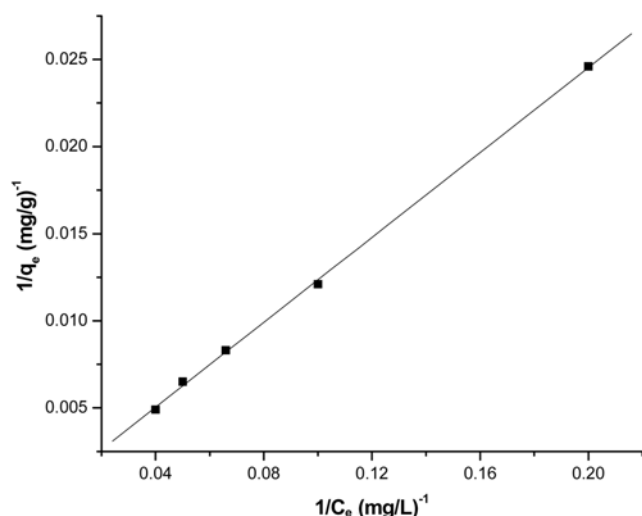
Fig. 7. Langmuir plot ($1/q_e$ vs C_e). Conditions, electrolyte pH: 6.5, electrolyte temperature: 305 K, current density: 0.06 A dm^{-2}.

Table 3. Langmuir constants for the adsorption of iron at temperature 305 K and pH 6.5

Concentration of iron (mg/L)	q_m (mg/g)	K_a (L/mg)	R_L
5			0.9864
10			0.9732
15	5912.40	0.001388	0.9604
20			0.9479
25			0.9357

that of other adsorbents studied [28]. The lower value of the removal efficiency is due to the pH of the solution, which was found to be >8.0. This condition is not favorable for the adsorption of iron (Fig. 3).

The essential characteristics of the Langmuir isotherm can be expressed as the dimensionless constant R_L [32],

$$R_L = 1/(1+bc_o) \qquad (15)$$

where, R_L is the equilibrium parameter, C_o is the initial iron concentration and b is the Langmuir constant. The R_L values indicate the type of isotherm: irreversible ($R_L=0$), favorable ($0<R_L<1$), linear ($R_L=1$) or unfavorable ($R_L>1$) [33]. In present study, the R_L values were found to be between 0 and 1 for all the concentrations of iron studied (5-25 mg/L). The results are presented in Table 3.

6. Effect of Temperature

The amount of iron adsorbed on the adsorbent increases by increasing the temperature, indicating the process to be endothermic [34]. The diffusion coefficient (D) for the intraparticle transport of an iron species into the adsorbent particles has been calculated at different temperature by [32],

$$t_{1/2} = 0.03 \, (r_o^2/D) \qquad (16)$$

where $t_{1/2}$ is the time of half adsorption (s), r_o is the radius of the adsorbent particle (20×10^{-4} cm), and D is the diffusion coefficient in cm^2/s. For all chemisorption systems the diffusivity coefficient should be 10^{-5} to 10^{-13} cm^2/s [35]. In the present work, D is found to be in the range of 10^{-10} cm^2/s. The pore diffusion coefficient (D) values for different initial concentrations of iron and temperature are pre-

Table 4. Pore diffusion coefficients for the adsorption of iron at temperature 305 K and pH 6.5

Initial iron concentration (mg/L)	Pore diffusion constant $D \times 10^{10}$ (cm^2/s)
5	4.100
10	6.005
15	4.300
20	2.510
25	5.920

Table 5. Pore diffusion coefficients for the adsorption of iron at pH 6.5 and 25 mg/L

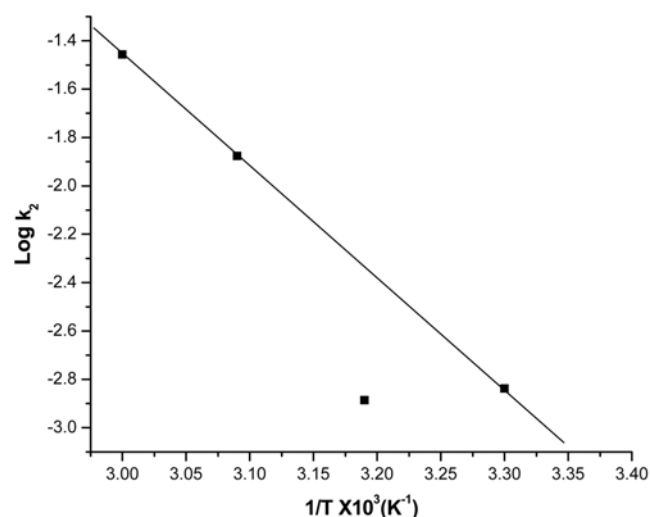| Temperature (K)	Pore diffusion constant $D \times 10^{10}$ (cm^2/s)
305	5.920
313	4.810
323	7.680
333	7.840

Fig. 8. Plot of log k_2 and 1/T. Conditions, electrolyte pH: 6.5, concentration of iron: 25 mg/L, current density: 0.06 A dm^{-2}.

sented in Table 4 and Table 5, respectively, and it is found that the present study follows the chemisorption system.

To find the energy of activation for the adsorption of iron, the second-order rate constant is expressed in the Arrhenius form [36],

$$\log k_2 = (\log k_o) - \frac{E}{2.303RT} \qquad (17)$$

where k_o is the constant of the equation (g min/mg), E is the energy of activation (J/mol), R is the gas constant (8.314 J/mol K), and T is the temperature in K. Fig. 8 shows that the rate constants vary with temperature according to Eq. (17). The activation energy (42.39 kJ/mol) is calculated from the slope of the fitted equation. The free energy change is obtained from the following relationship:

$$\Delta G^0 = -RT \ln b \qquad (18)$$

where ΔG^0 is the change in free energy (kJ/mol), b is the equilibrium constant, R is the gas constant and T is the temperature in K.

Table 6. Thermodynamic parameters for the adsorption of iron

Temperature (K)	ΔG^o (kJ/mol)	ΔH^o (kJ/mol)	ΔS^o (kJ/mol K)
305	−06.48		
313	−14.57	137.9	41.74
323	−28.76		
333	−42.35		
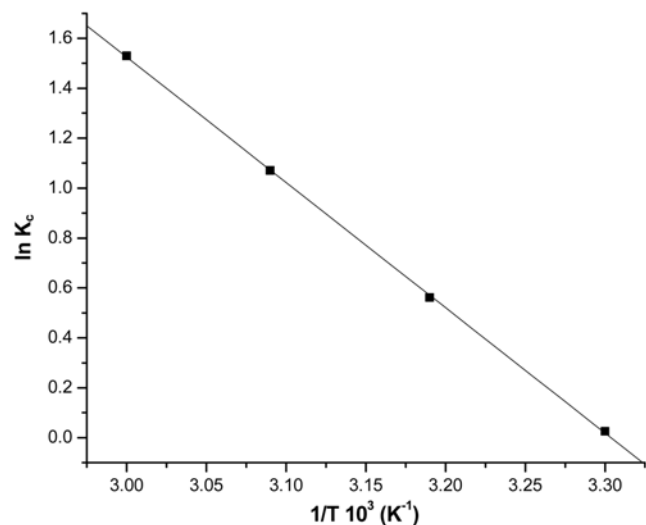
Fig. 9. Plot of ln K_c and 1/T. Conditions, electrolyte pH: 6.5, concentration of iron: 25 mg/L, current density: 0.06 A dm^{-2}.

Table 7. Comparison between the experimental and calculated q_e values for initial iron concentration 25 mg/L in second-order adsorption isotherm at various temperatures (pH 6.5)

Temperature (K)	q_e Experimental (mg/g)	k_2 (min g/mg)	q_e Calculated (mg/g)	R^2
305	202.58	0.0014	201.00	0.9998
313	208.25	0.0093	207.93	0.9994
323	214.65	0.0133	214.42	0.9999
333	215.43	0.0350	216.45	0.9999

(a)
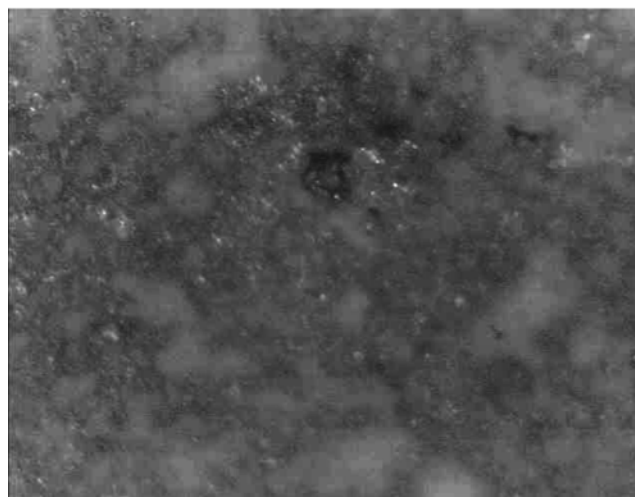
(b)

Fig. 10. Microscopic image of the anode (a) before, and (b) after treatment.

The ΔG^0 values are presented in Table 6. From the table it is found that the negative value of ΔG^0 indicates the spontaneous nature of adsorption.
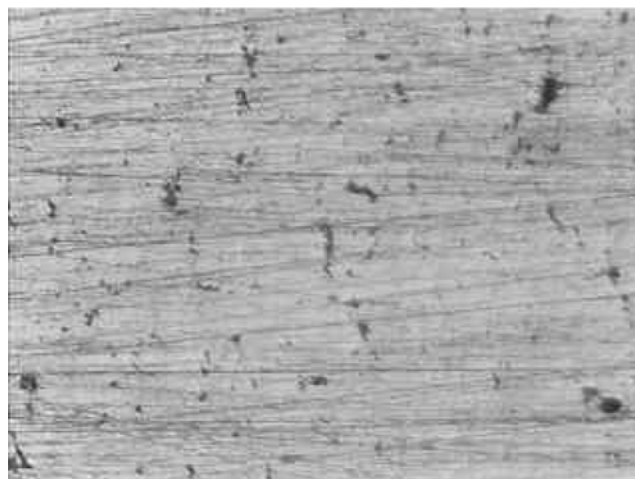
Other thermodynamic parameters such as entropy change (ΔS^0) and enthalpy change (ΔH^0) were determined by using the van't Hoff equation,

$$\log K_c = \frac{\Delta S^0}{2.303R} - \frac{\Delta H^0}{2.303RT} \tag{19}$$

The enthalpy change (ΔH^0) and entropy change (ΔS^0) were obtained from the slope and intercept of the van't Hoff linear plots of ln K_c versus 1/T (Fig. 9). A positive value of enthalpy change (ΔH^0) indicates that the adsorption process is endothermic in nature, and the negative value of change in free energy (ΔG^0) shows the spontaneous adsorption of iron on the adsorbent. Positive values of entropy change show the increased randomness of the solution interface during the adsorption of iron on the adsorbent (Table 6). Enhancement of the adsorption capacity of the electrocoagulant (aluminum hydroxide) at higher temperatures may be attributed to the enlargement of the pore size and or activation of the adsorbent surface. Using the Lagergran rate equation, first-order rate constants and correlation coefficients were calculated for different temperatures (303-333 K). The calculated 'q_e' values obtained from the first-order kinetics do not agree with the experimental 'q_e' values. The second-order kinetics model shows that the calculated 'q_e' values agree with the experimental values (Table 7). This indicates that the adsorption follows the second-order kinetic model at different temperatures used in this study. From the table, it is found that the rate constant 'k_2' increased with increasing the temperature from 305 to 333 K. The increase in adsorption may be due to a change in pore size upon increasing in kinetic energy of the iron species and the enhanced rate of intraparticle diffusion of the adsorbate.

Fig. 10(a) and (b) show the microscopic image of the anode before and after treatment. The microscopic image indicates the pres-

ence of ultrafine particles of micron size on the surface.

CONCLUSIONS

The results show that the maximum removal efficiency of 98.8% was achieved at a current density of 0.06 A dm^{-2} and a pH of 6.5 using aluminum alloy as the anode and stainless steel as the cathode. The aluminum hydroxide generated in the cell removes the iron present in the water and reduces the iron concentration to 0.2 mg/L, making it drinkable. The results indicate that the process can be scaled up to higher capacity. The adsorption of iron preferably fitting the Langmuir adsorption isotherm suggests monolayer coverage of adsorbed molecules. The adsorption process follows second-order kinetics. Temperature studies showed that adsorption was endothermic and spontaneous.

ACKNOWLEDGMENTS

REFERENCES

1. B. Das, J. Talukdar, S. Sarma, B. Gohain, R. K. Dutta and A. C. Das, *Curr. Sci.*, **85**, 657 (2003).
2. D. B. Mahanta, N. N. Das and R. K. Dutta, *Indian J. Environ. Prot.*, **24**, 654 (2004).
3. R. Sharma, S. Shah and C. Mahanta, *Asain J. Water Environ. Pollut.*, **2**, 47 (2005).
4. N. Subba Rao, *Environ. Monit. Assess.*, **136**, 437 (2007).
5. WHO Guidelines for Drinking Water Quality, *Health criteria and other supporting information, 2nd edition (2)*, WHO, Geneva (1996).
6. *Council directive 98/83/EC on the quality of water intended for human consumption*, L330/32-L330/50, Official Journal of the European Communities (1998).
7. *Central pollution control board*, Ministry of Environment and Forests, http://www.cpcb.nic.in Government of India, Delhi.
8. K. Vaaramaa and H. J. Lehto, *Desalination*, **155**, 157 (2003).
9. R. Munter, H. Ojaste and J. Sutt, *J. Environ. Eng.*, **131**, 1014 (2005).
10. W. C. Andersen and T. J. Bruno, *Anal. Chim. Acta*, **485**, 1 (2003).
11. P. Berbenni, A. Pollice, R. Canziani, L. Stabile and F. Nobili, *Bioresour. Technol.*, **74**, 109 (2000).
12. H. A. Aziz, M. S. Yusoff, M. N. Adlan, N. H. Adnan and S. Alias, *Water Manage.*, **24**, 353 (2004).
13. D. Ellis, C. Bouchard and G. Lantagne, *Desalination*, **130**, 255 (2000).
14. B. Das, P. Hazarika, G. Saikia, H. Kalita, D. C. Goswami, H. B. Das, S. N. Dube and R. K. Dutta, *J. Hazard. Mater.*, **141**, 834 (2007).
15. B. Y. Cho, *Process Biochem.*, **40**, 3314 (2005).
16. D. W. Miwa, G. R. P. Malpass, S. A. S. Machado and A. J. Motheo, *Water Res.*, **40**, 3281 (2006).
17. E. Onder, A. S. Koparal and U. B. Ogutveren, *Sep. Purif. Technol.*, **52**, 527 (2007).
18. M. Ikematsu, K. Kaneda, M. Iseki and M. Yasuda, *Sci. Total Environ.*, **382**, 159 (2007).
19. C. Carlesi Jara, D. Fino, V. Specchia, G. Saracco and P. Spinelli, *Appl. Catals. B*, **70**, 479 (2007).
20. P. A. Christensen, T. A. Egerton, W. F. Lin, P. Meynet, Z. G. Shaoa and N. G. Wright, *Chem. Commun.*, **38**, 4022 (2006).
21. A. Carlos, M. Huitle and S. Ferro, *Chem. Soc. Rev.*, **35**, 1324 (2006).
22. C. Gabrielli, G. Maurin, H. Francy-Chausson, P. Thery, T. T. M. Tran and M. Tlili, *Desalination*, **201**, 150 (2006).
23. X. Chen, G. Chen and P. L. Yue, *Chem. Eng. Sci.*, **57**, 2449 (2002).
24. G. Chen, *Sep. Purif. Technol.*, **38**, 11 (2004).
25. N. Adhoum and L. Monser, *Chem. Eng. Process*, **43**, 1281 (2004).
26. M. Kobya, O. T. Can and M. Bayramoglu, *J. Hazard. Mater.*, **B100**, 163 (2003).
27. C. Namasivayam and K. Prathap, *J. Hazard. Mater.*, **123B**, 127 (2005).
28. G. Mckay and Y. S. Ho, *Water Res.*, **33**, 578 (1999).
29. C. Namasivayam and S. Senthil Kumar, *Ind. Eng. Chem. Res.*, **37**, 4816 (1998).
30. F. H. Uber, *Z. Phys. Chem.*, **57**, 387 (1985).
31. I. Langmuir, *J. Am. Chem. Soc.*, **40**, 1361 (1918).
32. L. D. Michelson, P. G. Gideon, E. G. Pace and L. H. Kutal, *US Department Industry, Office of Water Research and Technology Bulletin* (1975).
33. W. Nigussie, F. Zewgeb and B. S. Chandravanshi, *J. Hazard. Mater.*, **147**, 954 (2007).
34. S. Nayak Preeti and B. K. Singh, *Res. J. Chem. Environ.*, **11**, 23 (2007).
35. X. Y. Yang and A. D. Bushra, *Chemical Engineering Journal*, **83**, 15 (2001).
36. A. K. Golder, A. N. Samantha and S. Ray, *Sep. Purif. Technol.*, **52**, 102 (2006).